A HIGH-RESOLUTION ANTENNA DIAGNOSTICS TECHNIQUE FOR SPHERICAL NEAR-FIELD MEASUREMENTS

C. Cappellin[1-2], O. Breinbjerg[1], A. Frandsen[2]

[1] *Ørsted•DTU, Technical University of Denmark, DK-2800 Kgs. Lyngby, Denmark,*
Email: cca@oersted.dtu.dk, ob@oersted.dtu.dk

[2] *TICRA, Læderstræde 34, DK-1201 Copenhagen K, Denmark,*
Email: af@ticra.com

ABSTRACT

A new diagnostics technique for spherical near-field antenna measurements, that can provide a high spatial resolution of the reconstructed aperture field, is presented. This technique is realized by transforming the spherical wave expansion (SWE) of the radiated field into the corresponding plane wave expansion (PWE), recovering a significant part of the invisible region of the plane wave spectrum. Through the inverse Fourier transform (IFT), the field on a plane outside as well as inside the antenna minimum sphere is reconstructed, with a resolution that exceeds the limit of one half a wavelength provided by the traditional IFT of the far-field.

1. INTRODUCTION

Antenna diagnostics is a technique to detect and identify electrical and mechanical errors in an antenna through an inspection of its radiated near-field. So far, several techniques, commonly based on far-field, planar or spherical near-field measurements, have been developed, all presenting limitations in their practical and theoretical realization [1]-[2]. We propose a new antenna diagnostics technique for spherical near-field measurements to be implemented at the DTU-ESA Spherical Near-Field Antenna Test Facility located at the Technical University of Denmark [3]. The measurements carried out in the DTU-ESA Facility are based on the spherical wave expansion (SWE) of the field radiated by the antenna. This field expansion is mathematically valid in any source-free region of space outside the so-called "minimum sphere" of the antenna, the smallest sphere, centred at the origin of the coordinate system, which completely encloses the antenna. By knowing the field on the measurement sphere, the field can be evaluated on a new and smaller sphere, larger than the minimum sphere. This is the limit of the most common diagnostics techniques used for spherical near-field measurements. We propose a way to exceed this limit. The idea is to derive from the SWE of the radiated field the plane wave spectrum of the same field. Once the plane wave spectrum on a given z plane outside or inside the minimum sphere is calculated, the plane wave expansion (PWE) of the field on that z plane is known. This allows the aperture field to be computed as the inverse Fourier transform (IFT) of the spectrum. By evaluating the plane wave spectrum also in part of the invisible region, the achieved spatial resolution on the z plane can exceed the traditional value of half a wavelength, provided by the traditional techniques. The first step consists of obtaining the SWE coefficients from a spherical near-field measurement; second, the plane wave spectrum in the visible, as well as in part of the invisible region, is calculated. The inverse Fourier transform is later applied to obtain the field on the desired z plane close to the antenna. In this manuscript the theory behind the new technique will be described and analytical calculations as well as numerical simulations will be shown. Investigations on the number of spherical modes necessary for the PWE convergence, and the corresponding sampling density on the measurement sphere, will be presented. The influence of truncations in the inverse Fourier transform will be finally studied. All theoretical results are expressed in the S.I. rationalized system with $e^{-j\omega t}$ time dependence.

2. THEORY

We start by introducing the SWE of the electric field $\vec{E}$ radiated by a general antenna circumscribed by a minimum sphere of radius r_o. In any source-free region $r > r_o$ the field can be expressed as a weighted sum of spherical waves [4],

$$\vec{E}(\vec{r}) = \frac{k}{\sqrt{\eta}} \sum_{n=1}^{\infty} \sum_{m=-n}^{n} Q_{1mn}^{(3)} \vec{F}_{1mn}^{(3)}(\vec{r}) + Q_{2mn}^{(3)} \vec{F}_{2mn}^{(3)}(\vec{r}) \qquad (1)$$

where $Q_{1mn}^{(3)}$ and $Q_{2mn}^{(3)}$ are the expansion coefficients, that can be obtained from a spherical near-field measurement, and $\vec{F}_{1mn}^{(3)}(\vec{r})$ and $\vec{F}_{2mn}^{(3)}(\vec{r})$ are the power-normalized spherical vector wave functions. The medium intrinsic admittance is denoted by η, k is the wave number, and $\vec{r}$ is the position vector expressed as a function of the traditional spherical coordinates (r, θ,

φ). In practice, the n-summation of the SWE is truncated at $n = N$, N being usually equal to $N = kr_o+10$. The PWE of the same electric field in the spectral (k_x k_y)-domain valid for $z > z_o$, with z_o being the largest z-coordinate of the source region, is given by [5]

$$\vec{E}(x,y,z) = \frac{1}{2\pi}\int_{-\infty}^{\infty}\int_{-\infty}^{\infty}\vec{T}(k_x,k_y)\,e^{jk_z z}e^{j(k_x x+k_y y)}dk_x dk_y \quad (2)$$

where k_x, k_y, k_z are the cartesian components of the wave propagation vector $\vec{k}$ with $k_z = \sqrt{k^2 - k_x^2 - k_y^2}$.
In practice, the k_x, k_y, integrals are truncated at a finite value $\pm k_{x\,max}$ and $\pm k_{y\,max}$. The plane wave spectrum for a given z-coordinate is thus $\vec{T}(k_x,k_y)e^{jk_z z}$, and it can be derived by the inverse of Eq. 2 or, in terms of the current source, by [5]

$$\vec{T}(k_x,k_y) = \frac{1}{4\pi k k_z \eta}\vec{k}\times\left(\vec{k}\times\int_V \vec{J}(\vec{r})e^{j(k_x x+k_y y+k_z z)}dV\right) \quad (3)$$

It will now be shown how the SWE of Eq. 1 can be transformed into the PWE of Eq. 2. For this purpose we introduce the PWE valid for $z > 0$, in the spectral (α,β)-domain of the spherical vector wave functions as given by [6]-[7]

$$\vec{F}^{(3)}_{1mn}(\vec{r}) = \\ = \frac{(-j)^n}{2\pi\sqrt{n(n+1)}}\int_{-\pi C_+}^{\pi}\int \vec{Y}^m_n(\alpha,\beta)e^{jk\hat{s}\cdot\vec{r}}\sin\alpha\, d\alpha\, d\beta \quad (4)$$

$$\vec{F}^{(3)}_{2mn}(\vec{r}) = \\ = \frac{j(-j)^n}{2\pi\sqrt{n(n+1)}}\int_{-\pi C_+}^{\pi}\int \hat{s}\times\vec{Y}^m_n(\alpha,\beta)e^{jk\hat{s}\cdot\vec{r}}\sin\alpha\, d\alpha\, d\beta \quad (5)$$

with $\hat{s} = \sin\alpha\cos\beta\,\hat{x} + \sin\alpha\sin\beta\,\hat{y} + \cos\alpha\,\hat{z}$, $\beta \in [-\pi, \pi]$ and $\alpha \in C_+$, see Fig. 1.

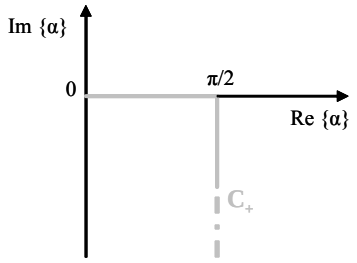

Fig. 1. Domain of the variable α with contour C_+.

The function $\vec{Y}^m_n(\alpha,\beta)$ is the vector spherical harmonics defined by

$$\vec{Y}^m_n(\alpha,\beta) = -j\frac{1}{\sqrt{2\pi}}\left(-\frac{m}{|m|}\right)^m\left(\frac{\partial}{\partial\alpha}\overline{P}^m_n(\cos\alpha)e^{jm\beta}\hat{\beta} + \right. \\ \left. -\frac{1}{\sin\alpha}\overline{P}^m_n(\cos\alpha)\,jm e^{jm\beta}\hat{\alpha}\right) \quad (6)$$

with $\overline{P}^m_n(\cos\alpha)$ being the normalized associated Legendre functions as defined by [4], $\hat{\alpha} = \cos\alpha\cos\beta\,\hat{x} + \cos\alpha\sin\beta\,\hat{y} - \sin\alpha\,\hat{z}$ and $\hat{\beta} = -\sin\beta\,\hat{x} + \cos\beta\,\hat{y}$. By substituting the PWE of the vector spherical harmonics, Eq. 4 and Eq. 5, into the SWE, Eq. 1, and by interchanging the order of integration and summation, since the double integral is uniformly convergent [6], the PWE of the electric field in the spectral (α,β)-domain, valid for every $z > r_o$, can be found as

$$\vec{E}(\vec{r}) = \frac{jk}{8\pi^2}\int_{-\pi C_+}^{\pi}\int \hat{E}(\hat{s})e^{jk\hat{s}\cdot\vec{r}}\sin\alpha\, d\alpha\, d\beta \quad (7)$$

where the spectrum complex amplitude $\hat{E}(\hat{s})$ is given by

$$\hat{E}(\hat{s}) = \sum_{n=1}^{\infty}\sum_{m=-n}^{n}\frac{(-j)^n 4\pi}{\sqrt{\eta}\sqrt{n(n+1)}}\left[Q^{(3)}_{2mn}\,\hat{s}\times\vec{Y}^m_n(\alpha,\beta) + \right. \\ \left. - jQ^{(3)}_{1mn}\vec{Y}^m_n(\alpha,\beta)\right] \quad (8)$$

Eq. 8 can thus be calculated from the knowledge of the SWE coefficients $Q^{(3)}_{1mn}$ and $Q^{(3)}_{2mn}$.
The spectrum in the spectral (α,β)-domain, $\hat{E}(\hat{s})e^{jkz\cos\alpha}$, can now be translated into the (k_x,k_y)-domain to obtain $\vec{T}(k_x,k_y)e^{jk_z z}$ by using the relation [7]

$$\vec{T}(k_x,k_y)e^{jk_z z} = \frac{1}{4\pi k_z}\hat{E}(\hat{s})e^{jk\cos\alpha z} \quad (9)$$

where (α,β) on the right hand side must be expressed as functions of the spectral variables k_x and k_y according to the relation $\hat{s} = \vec{k}/k$.
Having obtained the plane wave spectrum of Eq. 2 from the SWE of Eq. 1 on a given z plane, we can calculate the field on a new plane z_{new} being for example $z_{new} = z - \Delta L$, with $\Delta L > 0$, as depicted in Fig. 2, arriving at

$$\vec{E}(x,y,z_{new}) = \frac{1}{2\pi}\int_{-\infty}^{\infty}\int_{-\infty}^{\infty}\vec{T}(k_x,k_y)e^{jk_z(z-\Delta L)}e^{j(k_x x+k_y y)}dk_x dk_y \quad (10)$$

The obtained spatial resolution of the field is given by $\delta_x = \pi / k_{x\max}$, $\delta_y = \pi / k_{y\max}$ and thus can be achieved by selecting k_{xmax} and k_{ymax} appropriately in the SWE-to-PWE transformation.

We can therefore summarize the required steps of this antenna diagnostics technique as follows:

1. Evaluate the Q coefficients through a spherical near-field measurement of the SWE of the radiated field of the antenna under test (AUT).
2. Calculate the plane wave spectrum in the (k_x,k_y) domain on a given z plane, $z > r_o$, according to the SWE-to-PWE transformation, i.e. through Eqs. 8-9.
3. Back-transform the spectrum to a new z plane close to the antenna $z < r_o$.
4. Compute the field on the desired z plane as the inverse Fourier transform of the spectrum through Eq. 2.

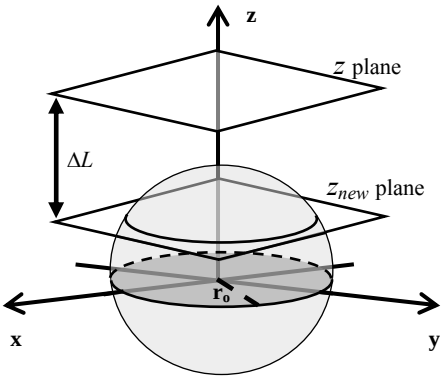

Fig. 2. Back- transformation of PWE from a z plane outside the minimum sphere to a new z plane inside the minimum sphere.

3. IMPLEMENTATION

3.1 Practical considerations

The new antenna diagnostics technique has been presented, but now some practical considerations have to be made.

- The z plane for the computation of the spectra as well as the fields has to be selected sufficiently close to the AUT to realize an efficient diagnostics.
- On that z plane, the extension of the spectral domain is chosen in order to ensure the desired spatial resolution of the aperture field, and to minimize the truncation error.
- The infinite series in n in Eq. 8 can be truncated to a finite number N, chosen sufficiently large to ensure the desired accuracy of the spectrum. This value can be different from the traditional $N = kr_o+10$.
- Given the required N, the sampling density on the measurement sphere is given by

$$\Delta\theta = \Delta\varphi = \frac{2\pi}{2N+1}$$

3.2 Test cases

Now that the steps of the new diagnostics technique are clear, we can illustrate the procedure by considering a simple antenna configuration. A set of four x-oriented Hertzian dipoles on the x-y plane, equally displaced at the distance r_o from the origin, are considered, see Fig. 3.

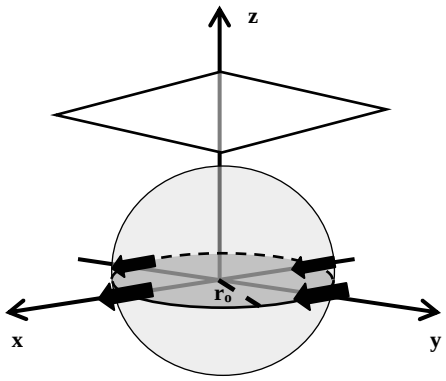

Fig. 3. Four x-oriented Hertzian dipoles on the x-y plane, the minimum sphere with radius r_o and the constant z plane.

The choice of this configuration is due to many factors. First of all, by locating the dipoles on the x-y plane, it is possible to investigate the effect of moving the z plane inside the minimum sphere. Second, for this antenna the Q coefficients can be calculated analytically avoiding the use of real measurements data, the use of which would have been premature at this point. Third, as it will be shown later, the radiated field contains arbitrarily high-order modes in n and m. Fourth, the analytical expression for the plane wave spectrum in the (k_x,k_y)-domain on the z plane, see Eq. 3, can be used as reference, since the dipole currents are known. In this way the truncation in the spectrum series of Eq. 8 can be analyzed. Fifth, the analytical expression of the radiated field can easily be calculated and used as a reference for the result of the IFT of the spectra.
Different value of r_o have been studied, here we present the results for $r_o = 2\lambda$, being r_o the dipole position as well as the minimum sphere radius. Also, we will consider $\Delta L = 1\lambda$, and thus the z planes $z = r_o + \Delta L = 3\lambda$ and $z_{new} = r_o - \Delta L = 1\lambda$.

For the calculation of the Q coefficients we refer to the results reported in [3; p.339]

$$Q_{1mn}^{(3)} = \frac{jkP}{\sqrt{8\pi n(n+1)\eta}}\left(-\frac{m}{|m|}\right)^m j_n(kr_o) \left.\frac{d\overline{P}_n^{|m|}(\cos\theta)}{d\theta}\left(\delta_{m,1}^4 - \delta_{m,-1}^4\right)\right|_{\theta=\pi/2} \tag{11}$$

$$Q_{2mn}^{(3)} = \frac{-kP}{\sqrt{8\pi n(n+1)\eta}}\left(-\frac{m}{|m|}\right)^m \left[\frac{n(n+1)}{kr_o} j_n(kr_o)\overline{P}_n^{|m|}(\cos\theta)\left(\delta_{m,1}^4 + \delta_{m,-1}^4\right) + \right. \tag{12}$$
$$+ \frac{1}{kr_o}\frac{d}{d(kr_o)}\{kr_o j_n(kr_o)\} m \frac{\overline{P}_n^{|m|}(\cos\theta)}{\sin\theta} \left.\left(\delta_{m,1}^4 - \delta_{m,-1}^4\right)\right]_{\theta=\pi/2}$$

In Eqs. 11-12, P denotes the dipole moment, $j_n(kr_o)$ is the spherical Bessel function, while $\delta_{m,\mu}^4$, $\mu = \pm 1$, is defined as

$$\delta_{m,\mu}^4 = \begin{cases} 1 & \bmod(m-\mu,4) = 0 \\ 0 & \text{otherwise} \end{cases} \tag{13}$$

By use of Eqs. 8-9-11-12, we can therefore solve the first and second steps of the procedure. To compare the obtained results with some reference values, we use Eq. 3

$$T_x = \frac{P}{2\pi k}\sqrt{\frac{\mu}{\varepsilon}}\left(\cos(k_x r_o) + \cos(k_y r_o)\right)\frac{k_x^2 - k^2}{k_z} \tag{14}$$

$$T_y = \frac{P}{2\pi k}\sqrt{\frac{\mu}{\varepsilon}}\left(\cos(k_x r_o) + \cos(k_y r_o)\right)\frac{k_x k_y}{k_z} \tag{15}$$

$$T_z = \frac{P}{2\pi k}\sqrt{\frac{\mu}{\varepsilon}}\left(\cos(k_x r_o) + \cos(k_y r_o)\right)k_x. \tag{16}$$

It is noted that a singularity for $k_z = 0$ ($k_x^2 + k_y^2 = 1$) is present in the x- and y-component. It can be proved that such a singularity will always be present at least in one of the spectrum components and that the necessary, but not sufficient, condition to avoid this singularity is that the antenna far-field pattern has a null for $\theta = \pi/2$.

3.2.1 Spectra computation

We choose a (k_x,k_y) domain equal to [-3k : 3k] × [-3k : 3k] and we sample it with 200×200 points. In Fig. 4 are the reference spectral components of Eqs. 14-15-16 and the one computed through Eqs. 8-9-11-12 with a truncation value of the n-series equal to $N = kr_o + 20$. All quantities are in linear scale and the selected z plane is $z = 3\lambda$. It is seen that all components, also those affected by singularity in k_z, are reconstructed, showing only a small difference in the amplitude of the order of 10^{-7}, see Fig. 5. If we decrease N, the difference increases: for $N = kr_o + 10$ it becomes of the order of 10^{-4}.

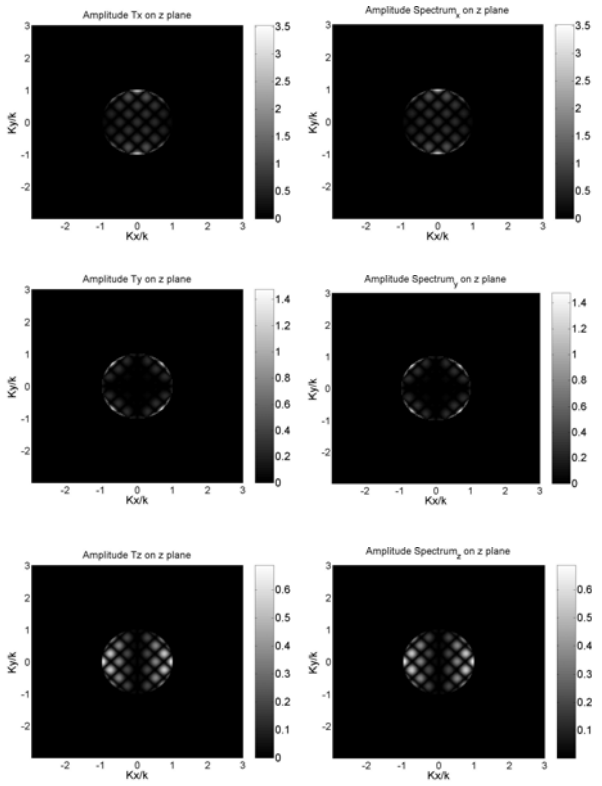

Fig. 4. Amplitude of the spectrum components on the plane $z = 3\lambda$: on the left the reference value of Eqs. 14-15-16, on the right the spectrum computed through the procedure for $N = kr_o + 20$.

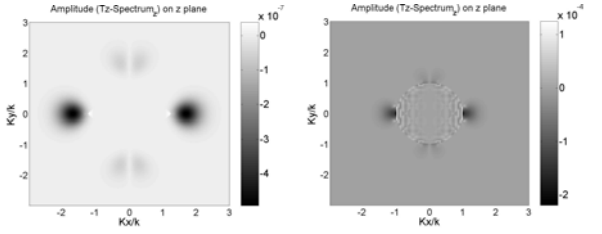

Fig. 5. Amplitude difference of T_z-spectrum$_z$ on $z = 3\lambda$, on the left for $N = kr_o + 20$, on the right for $N = kr_o + 10$.

For the same spectrum we compute also the phase: in Fig. 6 the result for the z component calculated with $N = kr_o + 20$ is shown. As we see, the phase is not reconstructed outside the visible region, even if we increase the number of sampling points. This happens to the other components as well. Although the very low amplitude of the spectrum in the invisible region, see

Fig. 4, means that an accurate reconstruction of the phase is not of high importance, we will briefly show how the phase reconstruction is influenced by the truncation number N.

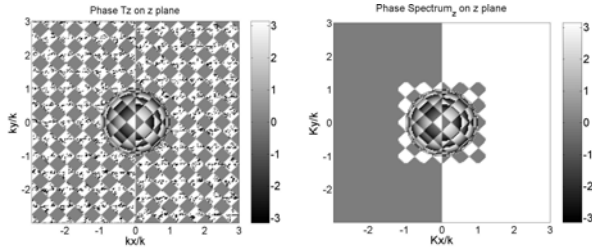

Fig. 6. Phase of the spectrum z component on $z = 3\lambda$: on the left the reference value of Eq. 16, on the right the spectrum computed through the procedure for $N = kr_o+20$.

We therefore increase N until $N = kr_o+50$ and we compute again the phase, see Fig. 7: now the phase is reconstructed inside the region $\pm 2k$ and the corresponding difference in amplitude is equal to 10^{-13}.

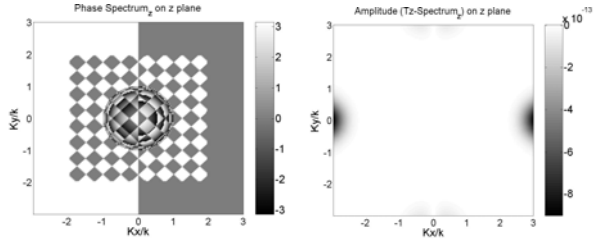

Fig. 7. Phase and amplitude of the spectrum z component on $z = 3\lambda$ for $N = kr_o+50$.

3.2.2 Fields computation

Now that the spectra calculated through the new procedure have been investigated, we can inverse Fourier transform them to compute the field on a z-plane outside and inside the minimum sphere. All figures are in linear scale.

a) Outside the minimum sphere on $z = 3\lambda$

The spectrum computed through Eqs. 8-9-11-12 is inverse Fourier transformed on the plane $z = 3\lambda$ with the truncation value $N = kr_o+10$. The (k_x,k_y)-domain is decreased to the value of $[-2k:2k]$, obtaining therefore a spatial resolution equal to $\lambda/4$. Just the z component will be analyzed to avoid difficulties in the IFT of functions with singularities. The results are shown in Figs. 8-9. The IFT results are in good agreement with the analytical reference field expression showing the same level of difference.

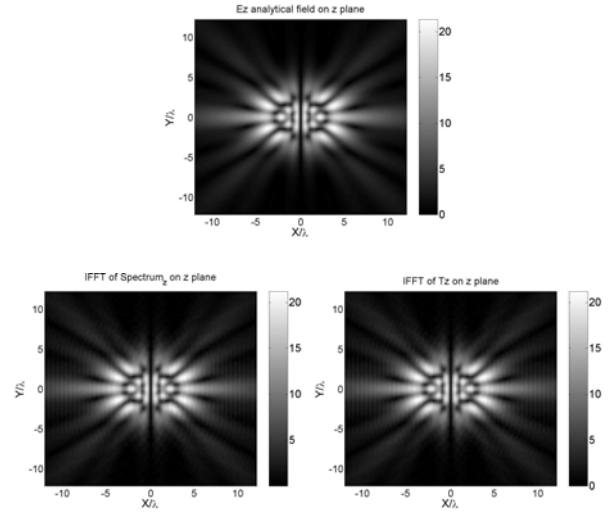

Fig. 8. Amplitude of the field z component on $z = 3\lambda$: on top the analytical value, on the left the IFT of the spectrum computed through the procedure for $N = kr_o+10$, on the right the IFT of the reference spectrum of Eq. 16.

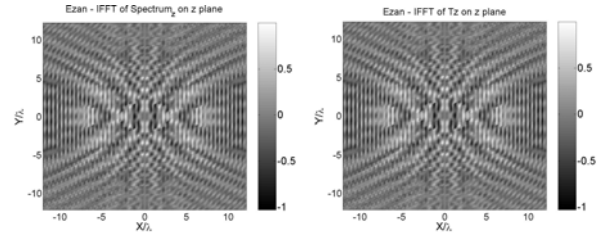

Fig. 9. Amplitude difference of the IFTs field z component, in respect of the analytical field on $z = 3\lambda$.

By looking at Fig. 9 we anyway see a difference in the IFT results of some 4% with respect to the analytical field, which is not quite satisfactory. Since both IFTs show the same difference value, the inaccuracy is not due to a too small number N of n-modes in the spectrum representation. The problem is also not due to a truncation in the spectral domain, since, see Fig. 4, the spectrum outside the visible region goes smoothly to zero and is not truncated to a finite value. The inaccuracy could therefore be due to an insufficient number of points in the spectral domain. To analyze this factor, we investigate therefore the results for 300×300 and 100×100 points, see the results in Fig. 10. The difference computed with 100×100 points is almost four times higher than the one with 200×200 points, while the one with 300×300 is half of the difference given by 200×200 points.

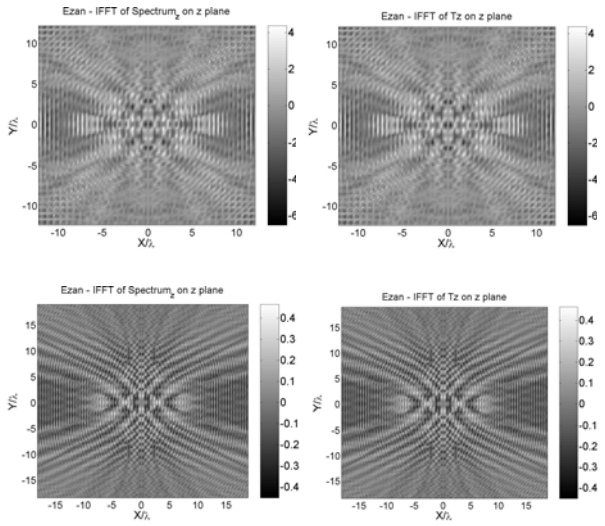

Fig. 10. Amplitude difference of the IFTs field z component, in respect of the analytical field on $z = 3\lambda$, on top with 100 sampling points, below with 300 sampling points. On the left the IFT of the spectrum computed through the procedure for $N = kr_o+10$, on the right the IFT of the reference spectrum of Eq. 16.

We choose therefore 300×300 as the number of sampling points in the (k_x,k_y)-domain and we now investigate the importance of the invisible region of the spectrum in the field reconstruction. In Figs. 11-12 are the inverse Fourier transforms of only the visible region of the spectra. Again the two IFTs look the same, but their differences with respect to the analytical value are almost twice the one in Fig. 10. On this z plane the knowledge of the invisible spectrum, besides providing a higher spatial resolution, can improve the accuracy of the field computation.

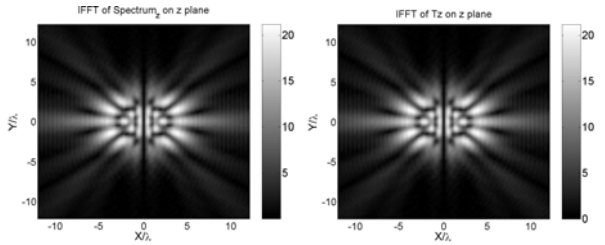

Fig. 11. Amplitude of the field z component on $z = 3\lambda$: on the left the IFT of the spectrum computed through the procedure for $N = kr_o+10$ (just visible region), on the right the IFT of the reference spectrum of Eq. 16 (just visible region).

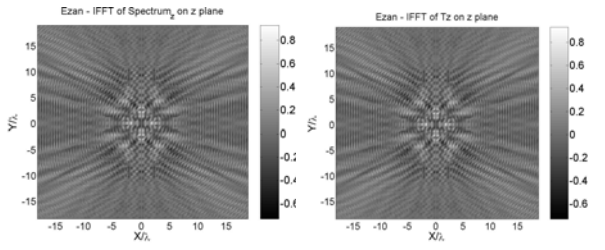

Fig. 12. Amplitude difference of the IFTs field z component (just visible region), in respect of the analytical field on $z = 3\lambda$.

b) Inside the minimum sphere on $z = 1\lambda$

Now the spectrum is back-propagated to a z-plane inside the minimum sphere and then inverse Fourier transformed.
The truncation value $N = kr_o+10$ is used and the results appear in Fig. 13. Inside the minimum sphere the considered number of modes is insufficient for a reconstruction of the field. The IFT of the spectrum calculated through the Q coefficients is totally different from both the reference analytical field and the IFT of the reference spectrum, while the IFT of the reference spectrum reconstructs the field with an even better accuracy than outside the minimum sphere, see Figs. 10-14.

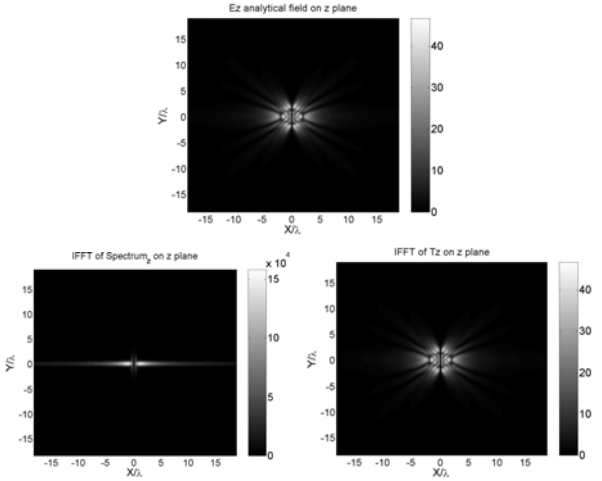

Fig. 13. Amplitude of the field z component on $z = 1\lambda$: on top the analytical value, on the left the IFT of the spectrum computed through the procedure for $N = kr_o+10$, on the right the IFT of the reference spectrum of Eq. 16.

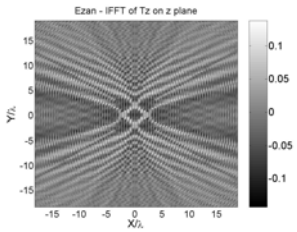

Fig. 14. Amplitude difference of the IFT of the reference spectrum of Eq. 16 in respect of the analytical field on $z = 1\lambda$.

To discriminate the source of error shown in Fig. 13 we inverse Fourier transform just the visible part of the spectrum obtained with $N = kr_o+10$. As we can see from Fig. 15, the result is now completely different meaning that the problem lies in the reconstruction of the invisible part of the plane wave spectrum. We compute therefore the spectrum at $z = 1\lambda$, see Figs. 16-17. The spectrum computed with $N = kr_o+10$ is totally

different from the reference spectrum, while by increasing N to the value $N = kr_o+50$, the spectrum is reconstructed with an accuracy of the order of 10^{-7}.

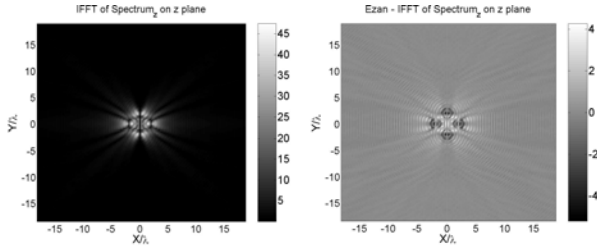

Fig. 15. Amplitude of the field z component on $z = 1\lambda$. On the left the IFT of the spectrum computed for $N = kr_o+10$, (just visible region), on the right its difference with the analytical value.

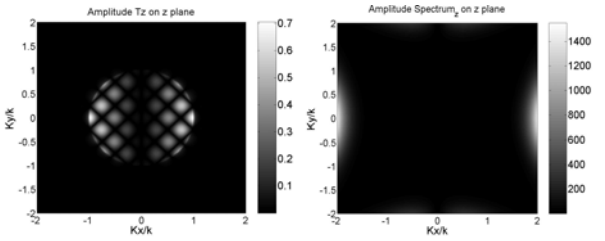

Fig. 16. Amplitude of the spectrum z component on the plane $z = 1\lambda$: on the left the reference value of Eq. 16, on the right the spectrum computed through the procedure for $N = kr_o+10$.

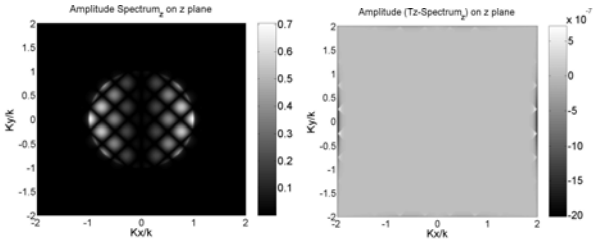

Fig. 17. Amplitude of the spectrum z component on the plane $z = 1\lambda$: on the left the spectrum computed through the procedure for $N = kr_o+50$, on the right the difference with the reference value of Eq. 16.

We therefore use $N = kr_o+50$ and we calculate again the IFT, see Fig. 18. Now the difference is almost equal to the one given by the IFT of the reference spectrum in Fig. 14. This shows that an accurate spectrum and aperture field can be obtained inside the minimum sphere if the correct truncation number in the n-series of Eq. 8 is considered.

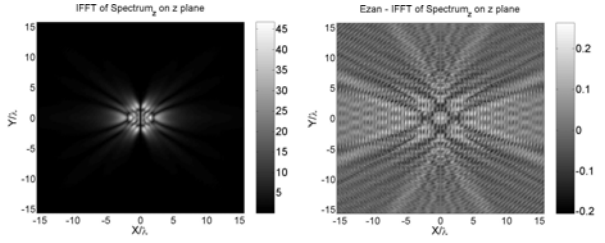

Fig. 18. Amplitude of the field z component on $z = 1\lambda$. On the left the amplitude of the IFT of the spectrum computed for $N = kr_o+50$, on the right its difference with the analytical value.

To complete our investigations, we show in Fig. 19 an example of aperture field reconstruction very close to the antenna, on the plane $z = 0.2\lambda$. The spectrum is computed with the truncation value $N = kr_o+50$ giving a difference in amplitude of almost 10%. This high value is due to an accuracy of the order of only 10^{-3} in the spectra reconstruction. The accuracy of the field can of course be decreased by increasing the value of N.

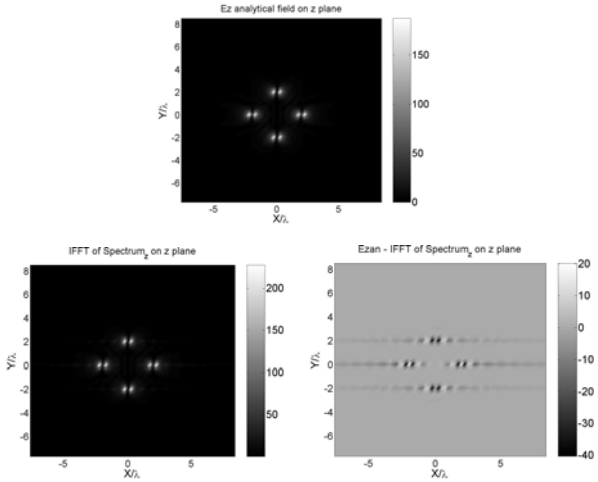

Fig. 19. Amplitude of the field z component on $z = 0.2\lambda$: on top the analytical value, on the left the IFT of the spectrum computed through the procedure for $N = kr_o+50$, on the right the difference with the analytical value.

4. CONCLUSIONS

A new diagnostics technique for spherical near-field antenna measurements, that can provide a high spatial resolution of the reconstructed aperture field, has been presented.

The plane wave spectrum is reconstructed in the visible as well as in part of the invisible region of the spectral domain. The achieved accuracy, on a z-plane outside and inside the antenna minimum sphere, is high being in excellent agreement with the analytical reference values. It has been shown that the n-series involved in the spectra expressions can be truncated to a finite number N.

Regarding the aperture field, the spatial resolution obtained here reaches the value of $\lambda/4$. It has been proved that an insufficient truncation value N in the spectrum can have different influences on the field computations. In particular, no errors are recovered when a spectrum with a low value of N is inverse Fourier transformed on a plane outside the minimum sphere. But when the field is computed inside the sphere, only a much higher value for N can reconstruct the field with good accuracy. The importance of the

knowledge of the invisible region of the spectrum in the field reconstruction has also been demonstrated.
Many investigations remain to be carried out in the future. In particular, for a given antenna of a certain size, a given z plane, a required accuracy and resolution, it is needed to establish a relation to determine the optimum N for the series of Eq. 8. Also, the IFT of spectra with a singularity will be optimized and more realistic antenna models will be investigated.

REFERENCES

1. Kaplan L., Hanfling J. D., Borgiotti G. V., *The Backward Transform of the Near-Field for Reconstruction of Aperture Field*, IEEE Trans. on Antennas and Propagation Soc. Symp. Dig., 764-767, 1979.

2. Joy E. B., Guler M. G., *High Resolution Spherical Microwave Holography*, IEEE Trans. on Antennas and Propagation, vol. 43, 464-472, 1995.

3. Homepage of the DTU-ESA Facility: http://www.emi.dtu.dk/research/afg/snf/SNF.html.

4. Hansen J. E., *Spherical Near-Field Antenna Measurements*, Peter Peregrinus Ltd. London 1988.

5. Hansen T. B., Yaghjian A. D., *Plane Wave Theory of Time-Domain Fields, Near-Field Scanning Applications*, IEEE PRESS, 1999.

6. Devaney A. J., Wolf E., *Multipole Expansion and Plane Wave Representations of the Electromagnetic Field*, Journal of Math. and Physics, Vol. 15, 234-244, February 1974.

7. Cappellin C., *Antenna Diagnostics in Spherical Near-Field Antenna Measurements by Plane Wave Expansion*, M. Sc. Thesis, Ørsted.DTU, Electromagnetic Systems, Technical University of Denmark, April 2004.